Photon Avalanche in Cs_2ZrBr_6:Os^{4+}

Markus Wermuth and Hans U. Güdel*

Contribution from the Department of Chemistry and Biochemistry, University of Bern, Freiestrasse 3, CH-3000 Bern 9, Switzerland

Received March 16, 1999

Abstract: The 15 K visible (VIS) upconversion-luminescence of Cs_2ZrBr_6:0.2% Os^{4+} upon excitation in the near-infrared (NIR) is presented and analyzed. Crystals of Cs_2ZrBr_6:0.2% Os^{4+} were synthesized and grown by the Bridgman technique. At 15 K VIS luminescence around 16000 cm^{-1} is induced by NIR excitation around 11400 and 13400 cm^{-1}. Due to the low maximum vibrational energy of 220 cm^{-1}, four excited states participate in the upconversion processes. A photon avalanche and a ground-state absorption/excited-state absorption sequence are identified as upconversion mechanisms by high-resolution upconversion-excitation spectra and by power-dependent and time-resolved measurements. The lifetimes of the excited states Γ_4 ($^3T_{1g}$), Γ_5 ($^3T_{1g}$), Γ_5 ($^1T_{2g}$), and Γ_1 ($^1A_{1g}$) at 15 K are 45 ms, 1.6 ms, 261 μs, and 8 μs, respectively. The dynamics of the upconversion are simulated with a rate-equation model.

1. Introduction

Upconversion (UC), i.e., photoexcitation at a long wavelength followed by luminescence at a shorter wavelength, is typically observed in compounds containing rare-earth ions.[1] Several upconversion mechanisms are well established in 4f systems. Common to all of them is the existence of long-lived intermediate states, which act as a storage reservoir for the pump energy. Subsequent emission from higher excited states can be induced radiatively by excited-state absorption (ESA) or nonradiatively by energy-transfer upconversion (ETU). The photon avalanche is an upconversion mechanism that contains both radiative and nonradiative steps. It is special in that it leads to strong upconversion luminescence at an excitation wavelength with a negligible ground-state absorption. There exist upconversion laser systems based on this pumping mechanism.[2−4] The photon avalanche was discovered in Pr^{3+}-doped crystals.[5] Among the rare-earth ions it was also observed for Nd^{3+}, Er^{3+}, and Tm^{3+}.[6] Avalanche systems exhibit very specific time and power dependencies, which can be simulated using rate-equation models.

Among the luminescent transition-metal ions in solids upconversion is an extremely rare phenomenon. As Kasha realized decades ago, there is usually only one metastable excited state with a sufficient lifetime to observe luminescence, i.e., the first excited state.[7] This is due to the stronger electron−phonon coupling than in rare-earth systems. Notable exceptions to Kasha's rule among the 3d ions are Ni^{2+} and Ti^{2+} in octahedral halide lattices.[8,9] Among these upconversion has been characterized and reported for Ni^{2+} and Ti^{2+}, and a photon avalanche upconversion process has been demonstrated for $CsCdCl_3$:

Ni^{2+}.[10] Recently we have extended our upconversion studies to 4d and 5d transition-metal ions and first results on Mo^{3+}, Re^{4+}, and Os^{4+} have already been published.[11,12]

Our motivation for exploring new near-infrared (NIR) to visible (VIS) upconversion systems among the transition-metal ions is 2-fold. A great deal of the upconversion work so far had a very strong physical emphasis, and it was almost exclusively devoted to lanthanide systems. Our aim is to add a chemical coordinate to this research. To our surprise, we find this field essentially unexplored. Transition-metal ions in a crystal environment exhibit both similarities and significant differences in their photophysical and spectroscopic properties to the rare-earth ions. As a consequence, we encounter new physical situations concerning competitions between radiative and nonradiative relaxation processes. It is our objective to use chemical variation to tune the light emission properties. This can only be done on the basis of a thorough understanding of the mechanisms governing excited-state dynamics. The present paper makes a significant step in this direction. Besides this fundamental driving force, NIR to VIS upconversion materials deserve attention because of their potential as UC phosphors and UC laser materials. Highly efficient and very compact semiconductor diode light sources are available for pumping the UC process. A number of lanthanide-doped laser materials have been developed which operate with the UC excitation principle.[13−17]

(1) Auzel, F. E. *Proc. IEEE* **1973**, *61*, 758.

(2) Lenth, W.; Macfarlane, R. M. *J. Lumin.* **1990**, *45*, 346.

(3) Koch, M. E.; Kueny, A. W.; Case, W. E. *Appl. Phys. Lett.* **1990**, *56*, 1083.

(4) Hebert, T.; Wannemacher, R.; Macfarlane, R. M.; Lenth, W. *Appl. Phys. Lett.* **1992**, *60*, 2592.

(5) Chivian, J. S.; Case, W. E.; Eden, D. D. *Appl. Phys. Lett.* **1979**, *35*, 124.

(6) Joubert, M. F.; Guy, S.; Jacquier, B.; Linares, L. *J. Appl. Spectrosc.* **1995**, *62*, 716.

(7) Kasha, M. *Discuss. Faraday Soc.* **1950**, *9*, 14.

(8) May, P. S.; Güdel, H. U. *J. Lumin.* **1990**, *47*, 19.

(9) Jacobsen, S. M.; Güdel, H. U. *J. Lumin.* **1989**, *43*, 125.

(10) Oetliker, U.; Riley, M. J.; May, P. S.; Güdel, H. U. *J. Lumin.* **1989**, *43*, 125.

(11) Wermuth, M.; Güdel, H. U. *Chem. Phys. Lett.* **1997**, *281*, 81.

(12) Gamelin, D. R.; Güdel, H. U. *J. Am. Chem. Soc.* **1998**, *120*, 12143.

(13) Johnson, L. F.; Guggenheim, H. J. *Appl. Phys. Lett.* **1971**, *19*, 44.

(14) Silversmith, A. J.; Lenth, W.; Macfarlane, R. M. *J. Opt. Soc. Am. A* **1986**, *3*, 128.

(15) Brede, R.; Danger, T.; Heumann, E.; Huber, G.; Chai, B. H. T. *Appl. Phys. Lett.* **1993**, *63*, 729.

(16) Trash, R. J.; Johnson, L. F. *J. Opt. Soc. Am. B* **1994**, *11*, 881.

(17) Sandrock, T.; Scheife, H.; Heumann, E.; Huber, G. *Opt. Lett.* **1997**, *22*, 808.

In the following we present the first extensive upconversion study on a 5d system: Os^{4+}-doped Cs_2ZrBr_6. The host lattice crystallizes in the cubic space group *Fm*3*m* and Os^{4+} substitutes for Zr^{4+} on octahedral sites. Whereas the absorption, luminescence, and MCD properties of this compound are well-known from the literature,[18-21] the upconversion field is still unexplored. The present study on $Cs_2ZrBr_6:Os^{4+}$ reveals quite unexpectedly the features of a photon avalanche. The upconversion behavior observed under different excitation wavelengths and by varying the excitation power is simulated by a rate-equation model including five electronic energy levels.

2. Experimental Section

2.1. Synthesis. Cs_2OsBr_6 was prepared from OsO_4 (Heraeus 99.9%) by reduction with HBr (Merck 47% pa) followed by precipitation with CsBr (Merck 99.5% suprapur).[22] The dark red product was dried under vacuum. With use of stoichiometric amounts of vacuum-dried CsBr (Merck 99.5% suprapur) and sublimed $ZrBr_4$ (Cerac 99.8%) crystals of Cs_2ZrBr_6 were grown in evacuated silica ampules by the Bridgman technique. Some remaining black impurities were removed before using the crystalline material to grow the Os^{4+}-doped crystal by the Bridgman technique. The resulting dark red crystal was cut into plates using a diamond saw and the surfaces were polished. With ICP mass spectrometry (inductively coupled plasma) an actual Os^{4+} concentration of 0.2% was determined for the sample used in the spectroscopic experiments.

All the handling of the starting materials and of the resulting crystals was carried out under nitrogen.

2.2. Spectroscopy. The samples were either enclosed in a copper cell or sealed in silica ampules, filled with 400 mbar helium for heat dissipation. Cooling was achieved with a closed-cycle cryostat (Air Products) for absorption measurements or with the helium-gas flow technique for luminescence experiments.

Absorption spectra were recorded on a Cary 5e (Varian) or a FT-IR spectrometer (Perkin-Elmer 1720×). Upconversion-luminescence spectra were obtained by using an argon-ion laser (Spectra Physics 2060-10 SA) pumped Ti:sapphire laser (Spectra Physics 3900 S). Wavelength control was achieved by an inchworm driven (Burleigh PZ 501) birefringent filter. The laser beam was focused ($f = 50$ mm) on the crystal. The excitation power was always measured in front of this lens. The sample luminescence was dispersed by a 0.85 m double monochromator (Spex 1402) and detected by a cooled photomultiplier tube (RCA 31034), using a photon counting system (Stanford Research 400).

Rectangular excitation pulses were generated by passing the laser beam through an acousto-optic modulator (Coherent 305) connected to a synthesized function generator (Stanford Research DS 345). For the lifetime determination of Γ_1 ($^1A_{1g}$) the frequency-doubled output of a Nd:YAG (yttrium aluminum garnet) laser (Quanta Ray DCR 3, 20 Hz) was used as the excitation source. The lifetime of Γ_5 ($^1T_{2g}$) was determined after pulsed excitation with the Raman shifted output (Quanta Ray RS-1, H_2 340 psi) of a dye laser (Lambda Physik FL 3002, Pyridin 1 in methanol) pumped with the frequency doubled Nd:YAG laser. The sample luminescence decay was detected with a red-sensitive photomultiplier (Hamamatsu 3310-01) and recorded with a multichannel scaler (Stanford Research 430). Luminescence spectra were corrected for the sensitivity of the detection system. They are displayed as photon counts versus energy. The data were analyzed using Igor (Wave Metrics).

(18) Inskeep, W. H.; Schwartz, R. W.; Schatz, P. N. *Mol. Phys.* **1973**, *25*, 805.
(19) Nims, J. L.; Patterson, H. H.; Khan, S. M.; Valencia, C. M. *Inorg. Chem.* **1973**, *12*, 1602
(20) Kozikowski, B. A.; Keiderling, T. A. *Mol. Phys.* **1980**, *40*, 477.
(21) Flint, C. D.; Paulusz, A. G. *Mol. Phys.* **1980**, *41*, 907.
(22) Brown, T. L.; McDugle, W. G.; Kent, L. G. *J. Am. Chem. Soc.* **1970**, *92*, 3645.
(23) Piepho, S. B.; Dickinson, J. R.; Spencer, J. A.; Schatz, P. N. *Mol. Phys.* **1972**, *24*, 609.
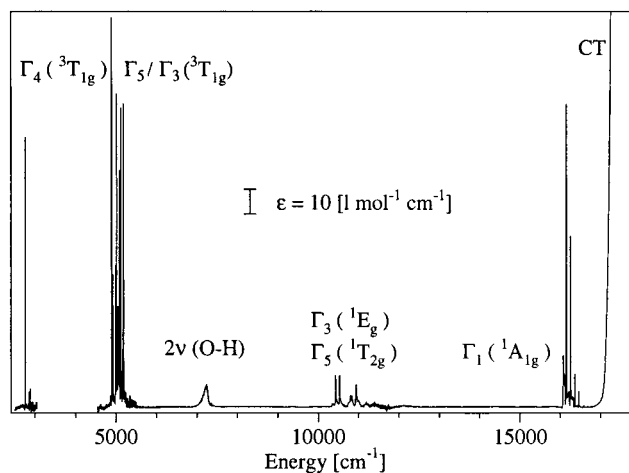

Figure 1. Survey absorption spectrum of $Cs_2ZrBr_6:Os^{4+}$ at 15 K in the NIR and VIS spectral region.
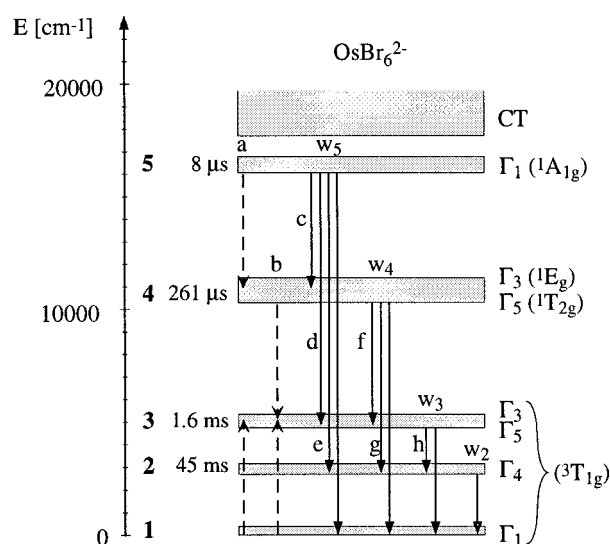

Figure 2. Energy-level scheme of $OsBr_6^{2-}$ with the relaxation processes included in the model calculation. Cross-relaxation steps are indicated with dashed arrows, whereas radiative and multiphonon relaxations at a single ion are represented by solid arrows. The designation of the processes and states is identical with the one used throughout the text and tables. The numbering of the states on the left-hand side refers to the model introduced in Section 4.2. The 15 K excited-state lifetimes are indicated.

3. Results

All the spectra presented here were measured on a crystal doped with 0.2% Os^{4+}. Figure 1 shows a survey absorption spectrum of $Cs_2ZrBr_6:Os^{4+}$ at 15 K. The sharp rise above 17000 cm^{-1} is to the first Br to Os charge-transfer (CT) excitation. According to the literature,[20] the four multiplets of sharp lines centered at about 2800, 5000, 10700, and 16200 cm^{-1} are assigned to the transitions Γ_1 ($^3T_{1g}$) → Γ_4 ($^3T_{1g}$), Γ_5/Γ_3 ($^3T_{1g}$), Γ_5 ($^1T_{2g}$)/Γ_3 (^1E_g), and Γ_1 ($^1A_{1g}$), respectively. All these d−d excited states belong to the ground-state electron configuration $(t_{2g})^4$, and that is why the absorption bands are sharp. The resulting energy-level scheme is depicted in Figure 2.

Excitation above 18000 cm^{-1} into the CT band leads to the luminescence spectrum shown in Figure 3. The transitions originating from the Γ_1 ($^1A_{1g}$) and Γ_5 ($^1T_{2g}$) states have a very different temperature dependence, as shown in the inset of Figure 3. Whereas the Γ_5 ($^1T_{2g}$) luminescence only shows a small decrease in intensity between 15 and 295 K, the Γ_1 ($^1A_{1g}$)
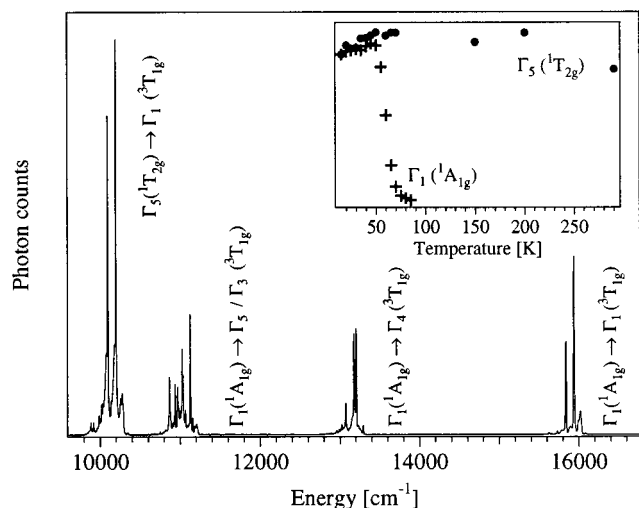
Figure 3. Luminescence spectrum of $Cs_2ZrBr_6:Os^{4+}$ at 15 K excited into the first CT band. The assignment is given on the right-hand side of the luminescence multiplets. The inset shows the integral of the luminescence bands Γ_1 ($^1A_{1g}$) $\rightarrow \Gamma_1$ ($^3T_{1g}$) and Γ_5 ($^1T_{2g}$) $\rightarrow \Gamma_1$ ($^3T_{1g}$), respectively, as a function of temperature, with the two data sets scaled to identical 15 K values.
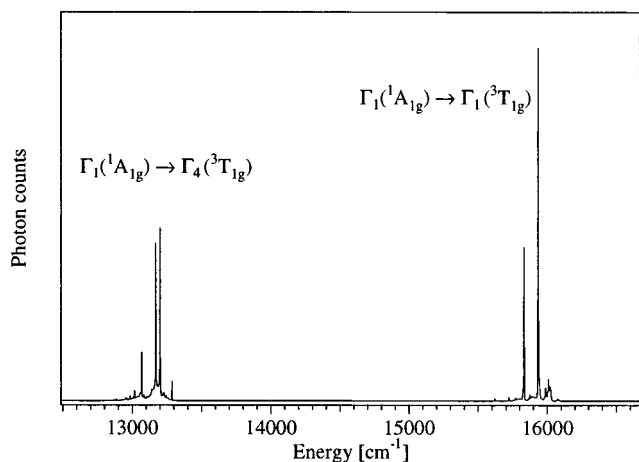

Figure 4. Upconversion-luminescence spectrum of $Cs_2ZrBr_6:Os^{4+}$ at 15 K excited at 11351 cm^{-1}.

luminescence intensity slightly increases up to 50 K and then drops very sharply and is completely quenched above 85 K. The slight increase in intensity is attributed to vibronic coupling.

Below 80 K red upconversion luminescence can be observed upon excitation in the near-infrared (NIR). Figure 4 shows the upconversion-luminescence spectrum obtained under 11351 cm^{-1} excitation at 15 K. The two multiplets around 13000 and 16000 cm^{-1} are assigned to Γ_1 ($^1A_{1g}$) $\rightarrow \Gamma_1$ ($^3T_{1g}$) and Γ_1 ($^1A_{1g}$) $\rightarrow \Gamma_4$ ($^3T_{1g}$), respectively, cf. Figure 2.

In Figure 5 the 15 K excitation spectrum monitoring the Γ_1 ($^1A_{1g}$) $\rightarrow \Gamma_1$ ($^3T_{1g}$) upconversion luminescence at 15900 cm^{-1} is compared with the corresponding 15 K absorption spectrum. The two spectra are completely different: Whereas excitation in the region of the most efficient ground-state absorption (GSA) only leads to very weak upconversion luminescence, the upconversion luminescence detected after excitation at 11351 and 13365 cm^{-1}, respectively, is more intense by 3 to 4 orders of magnitude. The solid arrows of insets a and b show the assignment of these latter two transitions to excited-state absorptions (ESA). The assignment of the upconversion induced by resonant ground-state absorption (GSA) is shown in inset c.
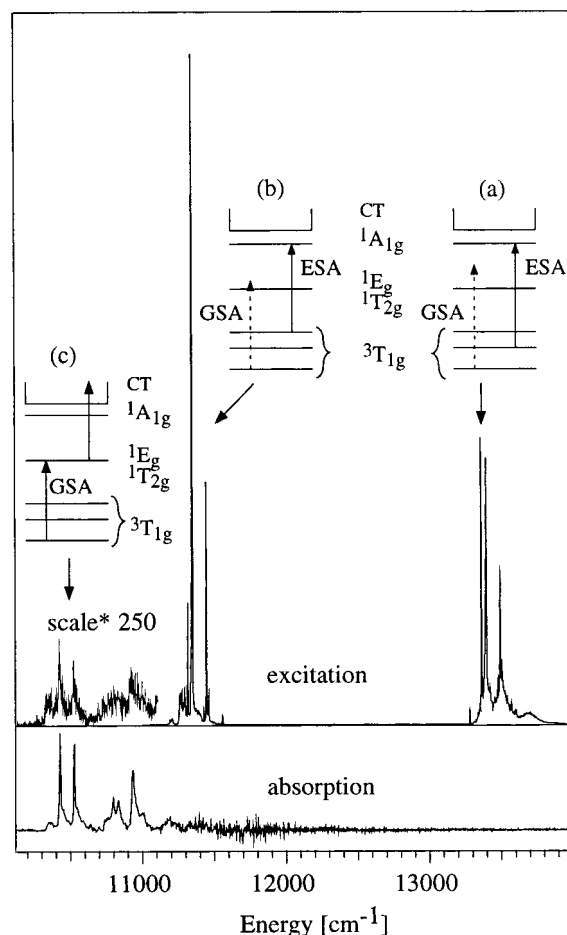

Figure 5. Upconversion-excitation spectrum of $Cs_2ZrBr_6:Os^{4+}$ at 15 K detecting the Γ_1 ($^1A_{1g}$) $\rightarrow \Gamma_1$ ($^3T_{1g}$) luminescence at 15933 cm^{-1}. The region below 11100 cm^{-1} is blown up by a factor of 250. The insets a, b, and c show the energies of the excitations as arrows in the schematic energy-level diagram of Os^{4+}. The 15 K absorption spectrum of the same spectral region is shown at the bottom.

Table 1. Comparison of Measured Decay-Rate Constants $1/\tau_{obs}$ of Excited States of $Cs_2ZrBr_6:Os^{4+}$ at 15 K and Calculated Radiative Decay-Rate Constants $1/\tau_{rad}$[a]

	$1/\tau_{obs}$	$1/\tau_{rad}$	k_{mp}	k_{cr}
Γ_1 ($^1A_{1g}$)	1.25×10^5	3.85×10^4		8.65×10^4
Γ_5 ($^1T_{2g}$)	3.83×10^3	2.82×10^3		1.00×10^3
Γ_5 ($^3T_{1g}$)	625	156	469	
Γ_4 ($^3T_{1g}$)	22.2	8.5	13.7	

[a] The difference is attributed to multiphonon relaxation k_{mp} and cross relaxation k_{cr}, respectively. All rate constants are given in s^{-1}.

It shows that CT states can easily be reached by adding up the energy of two NIR excitation photons.

The lifetimes τ_{obs} of all the long-lived excited states were experimentally determined at 15 K. The resulting decay-rate constants $1/\tau_{obs}$ are collected in Table 1. The lifetimes of 8 and 261 μs for the states Γ_1 ($^1A_{1g}$) and Γ_5 ($^1T_{2g}$), respectively, were obtained from luminescence-decay curves measured after direct pulsed excitation into these levels. The lifetime of Γ_5 ($^3T_{1g}$) was obtained in the following indirect way: Γ_1 ($^1A_{1g}$) $\rightarrow \Gamma_1$ ($^3T_{1g}$) luminescence was induced by rectangularly pulsed Γ_5 ($^3T_{1g}$) $\rightarrow \Gamma_1$ ($^1A_{1g}$) upconversion excitation at 11351 cm^{-1}. Special attention was given to the change of the upconversion-luminescence transient as a function of the duration of the dark period between two consecutive pulses. Figure 6 contains a whole series of transients for various excitation-interruption
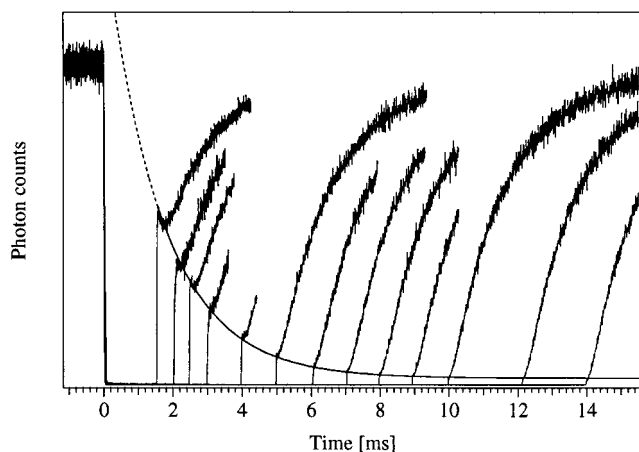
Figure 6. Time evolution of the Γ_1 ($^1A_{1g}$) → Γ_1 ($^3T_{1g}$) upconversion luminescence of Cs$_2$ZrBr$_6$:Os^{4+} excited at 11351 cm^{-1} with rectangular excitation pulses of 5 ms length. The dark period between two consecutive pulses was varied and is plotted on the *x*-axis. The smooth full line corresponds to a fit with an exponential function to the upconversion-luminescence intensity reached immediately after the switching on of the excitation. The dashed part of the curve represents the extrapolation to $t = 0$.

times in the range from 1.5 to 14 ms. These times are plotted on the *x*-axis, where $t = 0$ corresponds to the end of the preceding excitation pulse. The curves are all scaled to identical height of the steady-state upconversion luminescence reached before $t = 0$. The decay of each individual curve after $t = 0$ is very sharp, i.e., within the lifetime of Γ_1 ($^1A_{1g}$) of 8 μs, and the same is true for the rise of the upconversion luminescence in the first few microseconds after the resumption of the excitation. For the curves corresponding to short dark periods this sharp rise is even followed during a few 100 μs by a decrease in luminescence intensity before the slow rise toward the steady state begins again. As both the ESA Γ_5 ($^3T_{1g}$) → Γ_1 ($^1A_{1g}$) and the decay of Γ_1 ($^1A_{1g}$) are much faster than all the other relevant processes occurring in the system, the height of the sharp rise is a measure of the remaining population of Γ_5 ($^3T_{1g}$) at the onset of the next excitation pulse. Therefore the exponential solid line connecting the edges of the individual curves in Figure 6 corresponds to the population decay of Γ_5 ($^3T_{1g}$) as a function of time. From this exponential function, a Γ_5 ($^3T_{1g}$) lifetime $\tau = 1.6$ ms was extracted. Among the excited states not only Γ_5 ($^3T_{1g}$) has a non-zero population at $t = 0$, and hence the population evolution of Γ_5 ($^3T_{1g}$) during the first few 100 μs is affected by the relaxation of these higher excited states, leading to a strong deviation from an exponential population decay of Γ_5 ($^3T_{1g}$) in this first time period. This is why the steady-state upconversion luminescence at $t = 0$ in Figure 6 lies below the extrapolated dashed part of the exponential curve obtained from the least-squares fit to the data points after $t = 1.5$ ms.

The lifetime of Γ_4 ($^3T_{1g}$) was determined in an analogous way by exciting the UC luminescence at 13365 cm^{-1} corresponding to the ESA Γ_4 ($^3T_{1g}$) → Γ_1 ($^1A_{1g}$). Thus the extremely long lifetime $\tau = 45$ ms of Γ_4 ($^3T_{1g}$) was obtained.

In Figure 7, parts a and b, the Γ_1 ($^1A_{1g}$) → Γ_1 ($^3T_{1g}$) UC-luminescence intensity is depicted versus the measured laser power for the 13365 and 11351 cm^{-1} excitations, respectively. The insets again show the assignments of these two excitations. On a double logarithmic plot the curve for the 13365 cm^{-1} excitation appears as a straight line up to 1 mW with a slope of 2, corresponding to a quadratic power dependence. Then we observe a dramatic increase of the upconversion intensity and
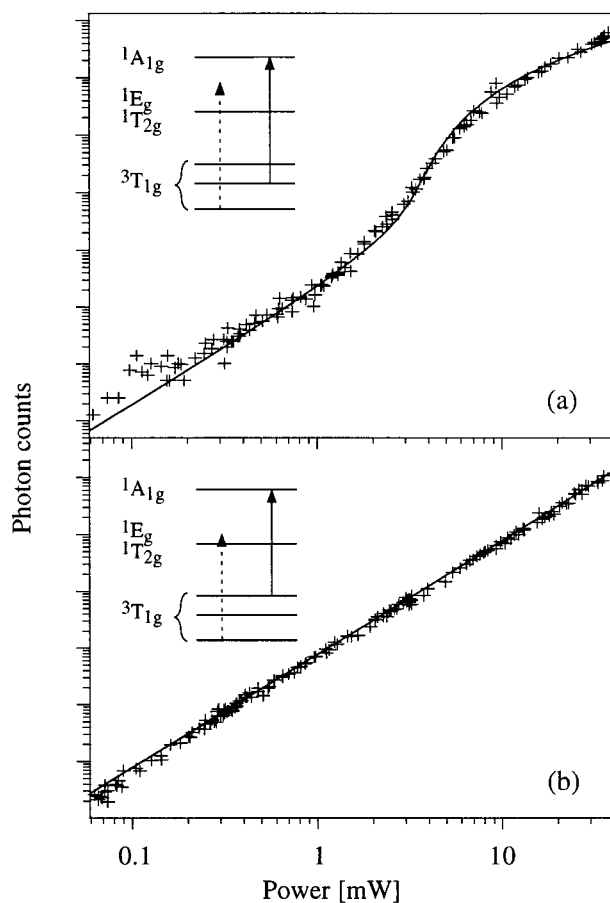

Figure 7. Double logarithmic plot of the Γ_1 ($^1A_{1g}$) → Γ_1 ($^3T_{1g}$) upconversion-luminescence intensity at 15 K versus the measured laser power obtained under 13365 (a) and 11351 cm^{-1} excitation (b), respectively. The smooth lines are calculated as described in Section 4.2.

the curve is approaching a slope of 4. After this threshold the curve is getting flatter again. Above 10 mW the slope is roughly 1.7. The power dependence of the UC-luminescence intensity excited at 11351 cm^{-1} is exactly quadratic over the whole power range of 3 orders of magnitude, leading to a straight line with slope 2 in the double logarithmic plot of Figure 7b. The calculation of the solid lines is described in Section 4.2.

Figures 8 and 9 show the time evolution of the UC-luminescence intensity excited with rectangular pulses at 13365 and 11351 cm^{-1}, respectively. The excitation starts at $t = 0$. The rise of the UC-luminescence intensity in the case of 13365 cm^{-1} excitation is extremely power dependent. Whereas the steady state for 1.6 mW excitation is reached after roughly 100 ms, the rise lasts for more than 1 s at an excitation power of 3.8 mW. 10 mW excitation power leads to an inflection point in the rise curve. For even higher excitation powers, the rise is getting faster again. In contrast, the time evolution of the UC-luminescence intensity for the 11351 cm^{-1} excitation is almost power independent, and the steady state is reached after roughly 10 ms, see Figure 9. The 50 mW transient is only slightly faster than the 5 mW transient. The calculation of the solid and dotted lines in Figures 8 and 9 is described in Section 4.2.

4. Discussion

4.1. Upconversion Mechanisms. The optical absorption, MCD, and luminescence properties of Os^{4+}-doped halide lattices have been reported.[18−21,23] Os^{4+} has a low-spin (5d)^4 electron configuration in all these octahedral complexes. Due to spin−
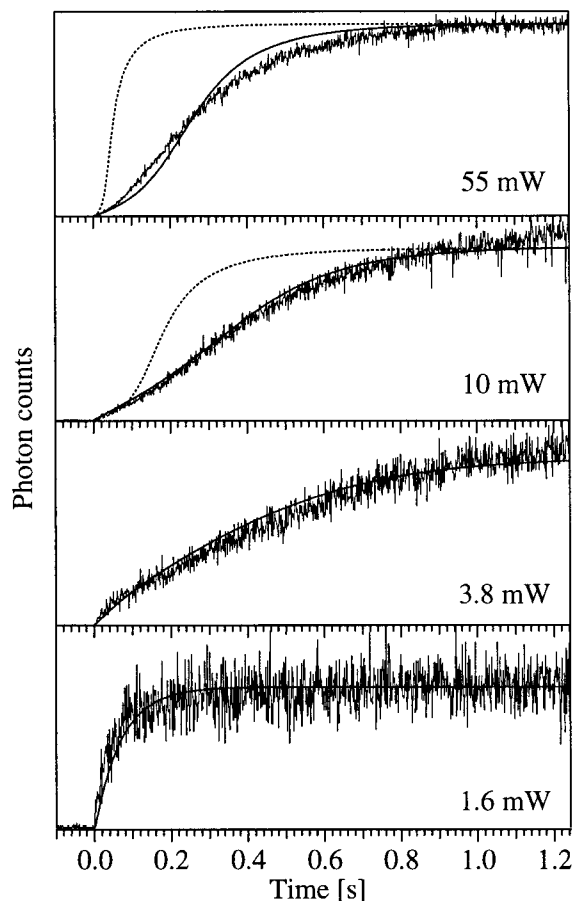
Figure 8. Rise of the upconversion-luminescence intensity after switching on the 13365 cm^{-1} excitation at $t = 0$ for four different excitation powers. The calculation of the solid and dotted lines is described in Section 4.2.

orbit coupling, the ground state $^3T_{1g}$ is split into four spinor components with a total spread of 5000 cm^{-1}, see Figure 2. The ligand field is so high in OsBr$_6^{2-}$ that all the excited states below 17000 cm^{-1} derive from the $(t_{2g})^4$ ground-state electron configuration. With the exception of the $\Gamma_1\,(^3T_{1g}) \rightarrow \Gamma_4\,(^3T_{1g})$ transition, which shows a magnetic dipole allowed electronic origin, most of the intensity of the absorption multiplets in Figure 1 lies in the vibronic origins involving t_{1u} and t_{2u} enabling modes. This proves the exact octahedral coordination of Os^{4+}, as expected from the cubic structure of the host lattice. Progressions in the a_{1g} mode built on the vibronic origins are very weak. For the $\Gamma_1\,(^3T_{1g}) \rightarrow \Gamma_1\,(^1A_{1g})$ transition a Huang–Rhys factor $S = 0.05$ is determined. The ground and the excited state thus have very similar equilibrium geometries as depicted in the configurational-coordinate diagram of Figure 10. This follows from the intraconfigurational nature of the transitions below 17000 cm^{-1}. As a consequence, multiphonon-relaxation processes between these states are greatly reduced, particularly in a chloride or bromide lattice with low vibrational energies, see Section 4.2. Alternative relaxation processes such as upconversion, cross-relaxation, and luminescence thus become competitive. In a preliminary account we have reported the observation of upconversion in the chloride analogue Cs$_2$ZrCl$_6$:Os^{4+}.[11]

Figure 4 clearly shows that NIR $\rightarrow$ VIS upconversion does occur in Cs$_2$ZrBr$_6$:Os^{4+} after excitation in the range between 10000 and 14000 cm^{-1}. The luminescent state is $\Gamma_1\,(^1A_{1g})$ at an energy of 16042 cm^{-1} and the two luminescence bands centered at 15900 and 13200 cm^{-1} correspond to the transitions
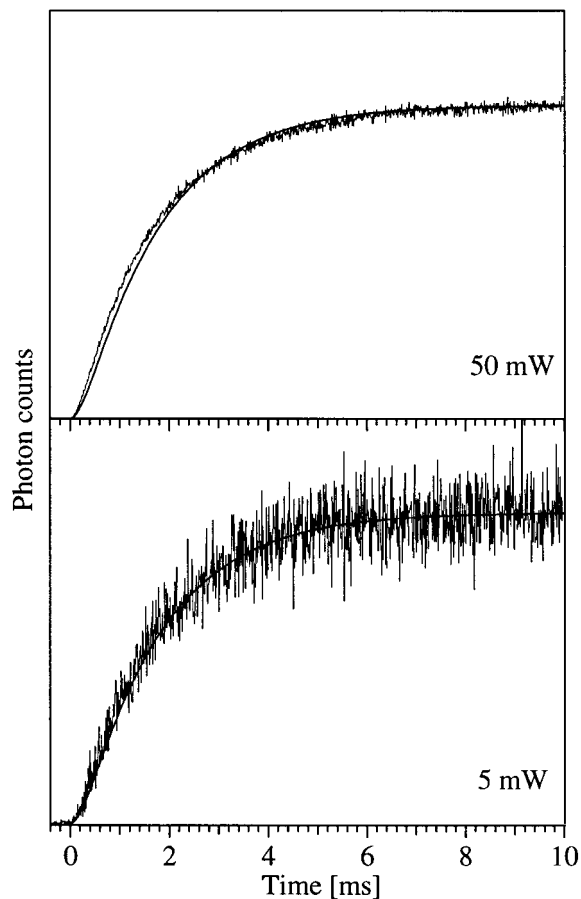

Figure 9. As in Figure 8, but for the 11351 cm^{-1} excitation.

$\Gamma_1\,(^1A_{1g}) \rightarrow \Gamma_1\,(^3T_{1g})$ and $\Gamma_1\,(^1A_{1g}) \rightarrow \Gamma_4\,(^3T_{1g})$, respectively. The upconversion luminescence is limited to temperatures below 80 K, because only at these cryogenic temperatures does the emitting state $\Gamma_1\,(^1A_{1g})$ relax to a significant extent through radiative processes, compare Figure 3. Above this temperature, thermally activated nonradiative relaxation via the energetically close lying CT states is getting predominant.

In the following, we will first outline the important upconversion mechanisms within the simple three-level model of Figure 11 before discussing the specific upconversion behavior of Cs$_2$ZrBr$_6$:Os^{4+}. Upconversion is always based on a sequence of processes, summing up the energies of several long wavelength excitation photons and leading to the emission of a photon at a shorter wavelength. In the first situation, denoted as GSA/ETU in Figure 11, the UC step is based on a nonradiative energy transfer (ETU) between two individual ions, both excited by ground-state absorption (GSA) to the intermediate level. Thus one of the ions is promoted to the upper excited state by the relaxation of the other ion to the lower state, see the dashed arrows in the left part of Figure 11. The energy-transfer step is based on multipolar or exchange interactions and can even occur in cases with considerable energy mismatch, because energy transfer can be phonon assisted. As the ETU step is most probable in cases with the highest intermediate-state population, the most intense upconversion luminescence is observed when the excitation source is tuned to the most efficient GSA. Therefore, the GSA/ETU mechanism is characterized by a close resemblance of upconversion excitation and corresponding absorption spectra.[11,12]

When the excitation source is tuned to an excited-state absorption (ESA) we can distinguish two situations, see Figure 11. If the cross section of the GSA step is significant at the
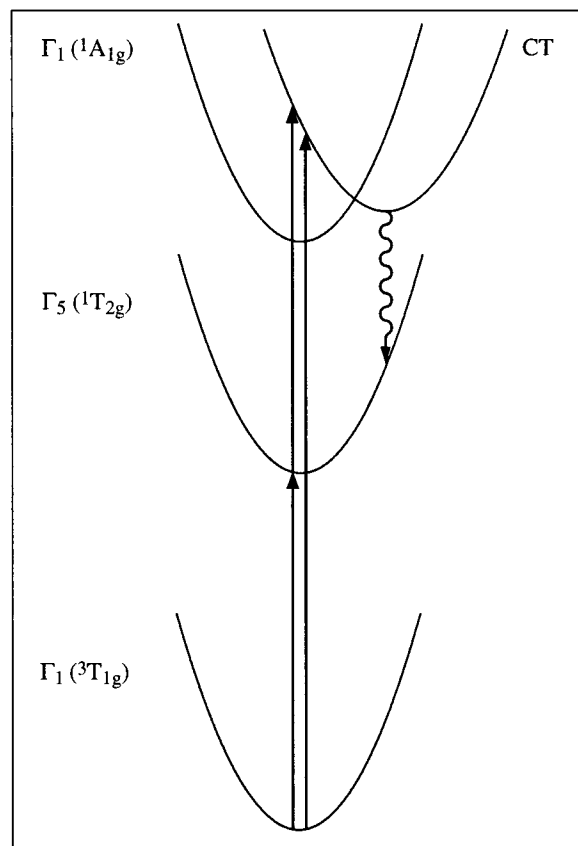
Figure 10. Schematic configurational-coordinate diagram of some selected states of $Cs_2ZrBr_6:Os^{4+}$. The solid arrows represent excitation, and the curly arrow represents an important multiphonon-relaxation process discussed in Section 4.1.
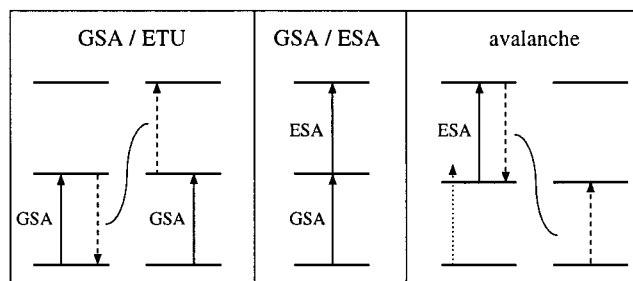

Figure 11. Schematic representation of the three fundamental upconversion mechanisms. GSA, ESA, and ETU stand for ground-state absorption, excited-state absorption, and energy-transfer upconversion, respectively. The dashed arrows represent nonradiative energy-transfer processes. The dotted arrow in the avalanche process shows negligible ground-state absorption at the laser energy.

excitation wavelength, an initial absorption to the intermediate state is followed by the ESA step to the higher excited state. For this GSA/ESA sequence the shape of the excitation spectrum is largely determined by the ESA step.[24]

If there is no significant GSA contribution at the ESA excitation energy, upconversion can occur via an avalanche mechanism in the following sequence: The avalanche starts with one single ion in the intermediate state. This initial excitation can arise by an extremely weak ground-state absorption, represented by the dotted arrow in Figure 11. The ion is then promoted to the upper excited state by ESA. By a cross-relaxation process, which is the reverse of an ETU process, the

ion in the upper excited state combines with a neighboring ground-state ion to create two ions in the intermediate state, see dashed arrows in the right part of Figure 11. This sequence of excitation and cross-relaxation steps continues and the population is exponentially built up, thus the term avalanche. As GSA only acts to initiate the process, the cross-relaxation has to compensate for all the population losses of the system, to get a self-sustaining process. The photon avalanche shows experimentally accessible fingerprints:[5,30] At a certain threshold excitation power, the UC-luminescence intensity strongly increases, and in the same power range the time evolution of the upconversion luminescence is characterized by an extremely long rise time. Above the threshold the rise period is getting shorter again and the rise curve is running through an inflection point. In $Cs_2ZrBr_6:Os^{4+}$ we can clearly distinguish these three mechanisms. Figure 5 with inset c shows that Γ_1 ($^3T_{1g}$) → Γ_5 ($^1T_{2g}$)/Γ_3 (^1E_g) GSA between 10300 and 11000 cm^{-1} leads to very weak upconversion luminescence. On the basis of evidence obtained from upconversion-luminescence decay curves measured after pulsed excitation at 10525 cm^{-1} both ESA and ETU contribute to this upconversion. The gain by 3 to 4 orders of magnitude in UC luminescence intensity when tuning the laser outside the GSA range (see Figure 5) is a clear indication that new mechanisms are at work. The two intense excitation multiplets around 11400 and 13400 cm^{-1} are the exact mirror image of the luminescence bands Γ_1 ($^1A_{1g}$) → Γ_5 ($^3T_{1g}$) and Γ_1 ($^1A_{1g}$) → Γ_4 ($^3T_{1g}$), respectively. They are readily assigned to the ESA processes Γ_5 ($^3T_{1g}$) → Γ_1 ($^1A_{1g}$) and Γ_4 ($^3T_{1g}$) → Γ_1 ($^1A_{1g}$), respectively, as depicted in insets a and b of Figure 5.

Whereas the assignment of the two bands to the ESA excitations is straightforward, we cannot differentiate between the GSA/ESA and the avalanche mechanism based on the excitation spectrum alone. The photon avalanche has to be considered as a valid mechanism for both excitations, the one around 11400 cm^{-1} as well as the one around 13400 cm^{-1}. In both cases ESA is much stronger than GSA: The ratio of the cross-sections ESA/GSA is around 60 for the 11351 cm^{-1} excitation and at least 200 for the 13365 cm^{-1} excitation, see Section 4.2.2. Cross-relaxation processes are possible as part of the feeding pathways of the intermediate levels Γ_5 ($^3T_{1g}$) and Γ_4 ($^3T_{1g}$): Cross relaxations of the type Γ_5 ($^1T_{2g}$) + Γ_1 ($^3T_{1g}$) → Γ_5 ($^3T_{1g}$) + Γ_5 ($^3T_{1g}$) and Γ_1 ($^1A_{1g}$) + Γ_1 ($^3T_{1g}$) → Γ_5 ($^1T_{2g}$) + Γ_5 ($^3T_{1g}$) can occur if some excess energy is released into the host lattice, see processes a and b drawn with dashed arrows in Figure 2.

Experimentally the typical avalanche fingerprints can be observed for the 13365 cm^{-1} excitation energy: The power dependence of the upconversion-luminescence intensity shows a threshold around 4 mW, see Figure 7a. The strong power dependence of the UC-luminescence rise curve after switching on the excitation is evident from Figure 8. The power of 3.8 mW leading to the slowest rise coincides with the steepest slope of the power dependence in Figure 7a. Thus the photon avalanche is unambiguously identified for this excitation wavelength.

The situation is completely different for the 11351 cm^{-1} excitation. The power dependence of the upconversion-luminescence intensity is exactly quadratic, corresponding to

(25) Förster, Th. *Ann. Phys. (Leipzig)* **1948**, *2*, 55.
(26) Dexter, D. L. *J. Chem. Phys.* **1953**, *21*, 836.
(27) Riseberg, L. A.; Moos, H. W. *Phys. Rev.* **1968**, *174*, 429.
(28) van Dijk, J. M. F.; Schuurmans, M. F. H. *J. Chem. Phys.* **1983**, *78*, 5317.
(29) Riedener, T.; Krämer, K. W.; Güdel, H. U. *Inorg. Chem.* **1995**, *34*, 2745.
(30) Collings, B. C.; Silversmith, A. J. *J. Lumin.* **1994**, *62*, 271.

(24) Krämer, K. W.; Güdel, H. U.; Schwartz, R. N. *Phys. Rev. B* **1997**, *56*, 13830.

an upconversion process involving the absorption of two pump photons, see Figure 7b. In addition, the rise of the upconversion luminescence is only moderately changing with increasing excitation power, see Figure 9. We conclude that, over the whole power range of 3 orders of magnitude, the feeding of the intermediate Γ_5 ($^3T_{1g}$) state, from which ESA to Γ_1 ($^1A_{1g}$) occurs, is dominated by GSA into very weak vibrational sidebands of Γ_5 ($^1T_{2g}$)/Γ_3 (^1E_g) at the 11351 cm^{-1} excitation energy, followed by the relaxation processes b and f·w_4 in Figure 2. The mechanism is thus a GSA/cross relaxation/ESA sequence.

The puzzling observation about the upconversion in Cs$_2$ZrBr$_6$: Os^{4+} is, that the excitations at 11351 and 13365 cm^{-1} lead to upconversion luminescence which is 3 to 4 orders of magnitude more intense than the one induced by resonant GSA excitation at 10525 cm^{-1}. This latter excitation appears to be favorable to induce upconversion because the CT states lying above 18000 cm^{-1} can easily be reached by absorption of a second photon or by an ETU process between two ions in the intermediate state Γ_5 ($^1T_{2g}$), see inset c of Figure 5. The extinction coefficients for the strongest CT ground-state absorptions are roughly 7000 L·mol^{-1}·cm^{-1} and thus 2 orders of magnitude higher than for the intraconfigurational absorptions below 17000 cm^{-1}. We can assume a similarly high cross-section for the excited-state transition Γ_5 ($^1T_{2g}$) → CT. This big ESA cross-section together with the resonant GSA should therefore dominate the upconversion behavior of the title compound. However, an excitation to the CT states does not necessarily lead to Γ_1 ($^1A_{1g}$) luminescence. As Figure 10 shows, the CT excitation can bypass the Γ_1 ($^1A_{1g}$) state by direct nonradiative relaxation to Γ_3 (^1E_g)/ Γ_5 ($^1T_{2g}$). From a comparison of the Γ_1 ($^1A_{1g}$) → Γ_1 ($^3T_{1g}$) and Γ_5 ($^1T_{2g}$) → Γ_1 ($^3T_{1g}$) luminescence-excitation spectra with the corresponding absorption spectrum in the energy range from 16000 to 21000 cm^{-1} a branching ratio of nonradiative relaxations at the crossing point of the Γ_1 ($^1A_{1g}$) and CT potentials of 1:100 in favor of relaxation into the CT minimum was obtained. The UC-luminescence efficiency after 10525 cm^{-1} excitation is adversely affected by this factor. The excitations at 11351 and 13365 cm^{-1}, on the other hand, elegantly avoid the CT states as they lead to direct excitation of Γ_1 ($^1A_{1g}$). A further advantage of these latter two excitations lies in the very long lifetimes of the states Γ_5 ($^3T_{1g}$) and Γ_4 ($^3T_{1g}$) from which the ESA processes to Γ_1 ($^1A_{1g}$) take place. Irrespective of the excitation wavelength, these intermediate states will always be more highly populated than Γ_5 ($^1T_{2g}$).

Above 50 K, however, the Γ_1 ($^1A_{1g}$) population shows a dramatic drop and completely vanishes above 80 K, see inset in Figure 3. With reference to Figure 10 we ascribe this to the very efficient nonradiative Γ_1 ($^1A_{1g}$) → CT transition, once the thermal energy is sufficient to overcome the energy barrier between the two states. The upconversion process after 11351 and 13365 cm^{-1} excitation is not thermally quenched, but a very efficient nonradiative relaxation pathway for the upconverted Γ_1 ($^1A_{1g}$) state becomes competitive above 50 K.

4.2. Dynamics of the Upconversion Processes. 4.2.1. Rate Equation Model. To explain the mechanistic differences of the upconversion luminescence excited at 13365 and 11351 cm^{-1}, respectively, the dynamics of the upconversion are analyzed with a rate-equation model. The processes to be considered can be separated into two classes, single-ion and multiion processes. Whereas the first class is independent of the spatial distribution of active ions, the efficiencies of the latter processes critically depend on the distances between active ions.[25,26] Therefore a distribution of rate constants should be attributed to a single energy-transfer process to account for the statistical distribution

of distances between dopant ions. As this would make a quantitative analysis intractable, we work with the approximation of mean rate constants in the following.

Among the single-ion processes, absorption of radiation and both radiative and nonradiative relaxation are important. Nonradiative relaxation is based on multiphonon processes. For the excited states below 17000 cm^{-1} we have concluded that ground and excited states have a similar equilibrium geometry. The situation is thus resembling f−f excited states in lanthanides, where the so-called energy-gap law is well established to estimate multiphonon-relaxation rate constants k_{mp}:[27]

$$k_{mp} = \beta e^{-\alpha p} \tag{1}$$

where α and β are parameters characteristic of the material and $p = \Delta E/\hbar\omega$ is the number of phonons of energy $\hbar\omega$ required to bridge the electronic energy gap ΔE. For f−f transitions in lanthanides multiphonon relaxation is usually competitive up to $p = 5$.[28,29] In OsBr$_6{}^{2-}$ multiphonon relaxation is expected to be important up to higher p values, as the 5d electrons are much more exposed to the environment and thus electron−phonon interactions are more important than for the f electrons of lanthanides. As a consequence the electronic factor in the expression for multiphonon relaxation is expected to be larger.

Among the multiion processes cross-relaxation is of major importance for the following analysis. As long as the excitation density is low, we only have to consider cross-relaxation processes with one of the two interacting ions in its electronic ground state.

The rate-equation model should simultaneously describe the upconversion behavior of Cs$_2$ZrBr$_6$:Os^{4+} observed at both excitation energies, 11351 and 13365 cm^{-1}. We therefore include all the excited states below 17000 cm^{-1} in the analysis. Due to the small energy gaps, fast multiphonon relaxation Γ_3 ($^3T_{1g}$) → Γ_5 ($^3T_{1g}$) and Γ_3 (^1E_g) → Γ_5 ($^1T_{2g}$) is assumed and the number of relevant states in our model is thus reduced to the following five: $\mathbf{1} \equiv \Gamma_1$ ($^3T_{1g}$), $\mathbf{2} \equiv \Gamma_4$ ($^3T_{1g}$), $\mathbf{3} \equiv \Gamma_5$ ($^3T_{1g}$)/Γ_3 ($^3T_{1g}$), $\mathbf{4} \equiv \Gamma_5$ ($^1T_{2g}$)/Γ_3 (^1E_g), $\mathbf{5} \equiv \Gamma_1$ ($^1A_{1g}$), see Figure 2.

The relaxation processes depicted in Figure 2 are included in the analysis. The same labeling of the processes is used in the rate equations below. Dashed and solid arrows represent cooperative and single-ion relaxations, respectively. Radiative and nonradiative processes are included in the latter. Due to the energetically regular spacing of the states $\mathbf{1}$, $\mathbf{3}$, $\mathbf{4}$, and $\mathbf{5}$, two cross-relaxations a and b, depicted with dashed arrows in Figure 2, are important. In this respect the system is very similar to the four-level system relevant for the avalanche system LaF$_3$: Tm^{3+}.[30] Cross-relaxations between two ions in excited states can be omitted as long as the excitation density is low. The total single-ion relaxation rate constants for the states $\mathbf{2}$, $\mathbf{3}$, $\mathbf{4}$, and $\mathbf{5}$ are symbolized by w_2, w_3, w_4, and w_5, respectively. The branching into the various lower states is characterized by the letters c, d, e, f, g, and h, as shown in Figure 2.

Finally, the excitation part included in the insets of Figure 5 has to be added to the model. For both excitations, 11351 and 13365 cm^{-1}, a weak GSA to state $\mathbf{4}$ is assumed. This excitation-rate constant is proportional to the excitation-photon flux density P and the cross-section σ_1. The ESA, proportional to the same P and to σ_2, connects $\mathbf{3}$ with $\mathbf{5}$ and $\mathbf{2}$ with $\mathbf{5}$ for the 11351 and 13365 cm^{-1} excitations, respectively. Apart from different GSA cross-sections σ_1, this change of the ESA is the only difference between the two excitation energies.

The following set of coupled rate equations describes the model in a mathematical way. N_i is the population density of state i. It is valid for the 13365 cm^{-1} excitation but can easily

be adapted to the 11351 cm^{-1} excitation:

$$\frac{dN_1}{dt} = -P\cdot\sigma_1\cdot N_1 - a\cdot N_1\cdot N_5 - b\cdot N_1\cdot N_4 + (1 - c - d - e)\cdot$$
$$w_5\cdot N_5 + (1 - f - g)\cdot w_4\cdot N_4 + (1 - h)\cdot w_3\cdot N_3 + w_2\cdot N_2$$

$$\frac{dN_2}{dt} = -P\cdot\sigma_2\cdot N_2 + e\cdot w_5\cdot N_5 + g\cdot w_4\cdot N_4 + h\cdot w_3\cdot N_3 - w_2\cdot N_2$$

$$\frac{dN_3}{dt} = a\cdot N_1\cdot N_5 + 2\cdot b\cdot N_1\cdot N_4 + d\cdot w_5\cdot N_5 + f\cdot w_4\cdot N_4 - w_3\cdot N_3$$

$$\frac{dN_4}{dt} = P\cdot\sigma_1\cdot N_1 + a\cdot N_1\cdot N_5 + c\cdot w_5\cdot N_5 - b\cdot N_1\cdot N_4 - w_4\cdot N$$

$$\frac{dN_5}{dt} = P\cdot\sigma_2\cdot N_2 - a\cdot N_1\cdot N_5 - w_5\cdot N_5 \qquad (2)$$

The above set of coupled rate equations can only be integrated numerically. Thus the time evolution of the populations N_i is obtained as a function of the parameter P representing the excitation-photon flux density. After a certain time the populations N_i reach their steady-state value and thus the P dependence of the population distribution under continuous-wave excitation is derived. To get a reasonable simulation of the upconversion processes induced by 11351 and 13365 cm^{-1} excitation, respectively, as many parameters as possible have to be fixed on the basis of independent experimental evidence.

4.2.2. Determination of Parameters. The observed decay-rate constants $1/\tau_{obs}$ in Table 1 are equal to the sum of radiative and nonradiative decay-rate constants for a given excited state. As radiative decay-rate constants $1/\tau_{rad}$ can be calculated from observed absorption oscillator strengths, the rate constants of the nonradiative processes $k_{nr} = k_{mp} + k_{cr}$, where k_{mp} and k_{cr} stand for multiphonon and cross-relaxation, respectively, are obtained as $k_{nr} = 1/\tau_{obs} - 1/\tau_{rad}$. In a two-level system the radiative lifetime τ_{rad} of the excited state is related to the oscillator strength f as follows:[31]

$$\tau_{rad} = \alpha \frac{\lambda_{eg}^2}{n[(n^2 + 2)/3]^2} \frac{g_e}{g_g} \frac{1}{f} \qquad (3)$$

α is a constant (1.5×10^4 s·m^{-2}), λ_{eg} is the average emission wavelength, g_g and g_e are the degeneracies of the ground an excited states, respectively, and n is the refractive index. In a multilevel system only the oscillator strengths of absorptions from the electronic ground state are available from absorption spectra, and therefore only the rate constants of radiative decays to the ground state are directly accessible. The rate constants of the radiative transitions to excited states can be obtained from the luminescence branching ratios, which correspond to the relative intensities of the luminescence bands originating from a given excited state. These branching ratios are equal to the ratios of the respective decay-rate constants and the sum of all these constants equals $1/\tau_{rad}$ for a specific state.

Table 1 shows that the decay-rate constants $1/\tau_{rad}$ calculated from absorption intensities using eq 3 are significantly smaller than $1/\tau_{obs}$, confirming the importance of nonradiative contributions to the relaxation of all the excited states below 17000 cm^{-1}.

(31) Imbusch, G. F.; Kopelman, R. In *Laser Spectroscopy of Solids*; Yen, W. M., Selzer P. M., Eds.; Springer-Verlag: Berlin, 1981.

Table 2. Parameters Used as Input Values for the Model Calculations^a

cross relaxations	a	8.65×10^4 s^{-1}
	b	1.00×10^3 s^{-1}
branching ratios	c	0.00
	d	0.29
	e	0.32
	f	0.50
	g	0.33
	h	0.75
single-ion	w_5	3.85×10^4 s^{-1}
relaxation-rate constants	w_4	2.82×10^3 s^{-1}
	w_3	625 s^{-1}
	w_2	22.2 s^{-1}

^{a} The designation of the processes is the same as in Figure 2.

According to the energy-gap law (eq 1) the quantity p, i.e., the energy gap in units of maximum energy vibrational quanta, is a relevant quantity. In Cs$_2$ZrBr$_6$ $\hbar\omega_{max} = 220$ cm^{-1}, and we get $p = 12, 9, 24,$ and 24 values for the electronic states Γ_4 (^{3}T$_{1g}$), Γ_5 (^{3}T$_{1g}$), Γ_5 (^{1}T$_{2g}$), and Γ_1 (^{1}A$_{1g}$), respectively. For $p = 24$ k_{mp} can be neglected, and the difference between $1/\tau_{rad}$ and $1/\tau_{obs}$ for Γ_1 (^{1}A$_{1g}$) and Γ_5 (^{1}T$_{2g}$) is fully attributed to the cross relaxations a and b, respectively, in Figure 2. The values for a and b are 8.65×10^4 and 1.00×10^3 s^{-1}, respectively, see Table 2.

At 15 K no cross-relaxations are possible to depopulate Γ_4 (^{3}T$_{1g}$) and Γ_5 (^{3}T$_{1g}$). Therefore the difference between $1/\tau_{rad}$ and $1/\tau_{obs}$ for these two states is completely due to multiphonon relaxation. For Γ_4 (^{3}T$_{1g}$) and Γ_5 (^{3}T$_{1g}$) k_{mp} values of 13.7 and 469 s^{-1} are obtained, see Table 1. These values are small as expected for energy gaps corresponding to p values of 12 and 9, respectively. But since the radiative decay-rate constants of Γ_4 (^{3}T$_{1g}$) and Γ_5 (^{3}T$_{1g}$) are extremely small, i.e., 8.5 and 156 s^{-1} (Table 1), respectively, these multiphonon-relaxation rate constants are significant, though.

The single-ion relaxation-rate constants w_5, w_4, w_3, and w_2 are equal to the respective sums $1/\tau_{rad} + k_{mp}$. Their values are listed in Table 2.

The values d and e of 0.29 and 0.32 for the transitions Γ_1 (^{1}A$_{1g}$) → Γ_5/Γ_3 (^{3}T$_{1g}$) and Γ_1 (^{1}A$_{1g}$) → Γ_4 (^{3}T$_{1g}$), respectively, were obtained from the relative luminescence intensities at 15 K, see Figure 3. As the transition Γ_1 (^{1}A$_{1g}$) → Γ_5 (^{1}T$_{2g}$)/Γ_3 (^{1}E$_g$) is very weak according to the literature,[21] the parameter c was set to zero. The Γ_1 (^{1}A$_{1g}$) → Γ_1 (^{3}T$_{1g}$) transition accounts for 39% of the total intensity from this emitting state. The parameters f and g were estimated from the luminescence spectra published by Flint et al.[21] and set to $f = 0.5$ and $g = 0.33$, respectively. The parameter h, finally, is equal to the ratio $k_{mp}/(1/\tau_{obs})$ of the state Γ_5 (^{3}T$_{1g}$), leading to $h = 0.75$, see Table 2.

The oscillator strengths of the ESA Γ_4 (^{3}T$_{1g}$) → Γ_1 (^{1}A$_{1g}$) and Γ_5 (^{3}T$_{1g}$) → Γ_1 (^{1}A$_{1g}$) are obtained from the respective radiative decay-rate constants. Thus the ratio of ESA to GSA cross-sections $\sigma_2/\sigma_1 = 60$ is obtained for the 11351 cm^{-1} excitation. At 13365 cm^{-1} we can only determine an upper limit for the GSA cross-section σ_1, leading to a lower limit for $\sigma_2/\sigma_1 > 200$. Apart from the product $P\cdot\sigma_1$ this ratio is the only variable parameter for the simulation of the 13365 cm^{-1} upconversion. For the 11351 cm^{-1} excitation $P\cdot\sigma_1$ is the only free parameter.

Guy et al. have shown the importance of taking into account the Gaussian intensity distribution of the excitation beam profile in the simulation of the photon avalanche.[32] This excitation inhomogeneity is extremely effective at excitation powers where the photon-flux density of the beam center lies above the

(32) Guy, S.; Joubert, M. F.; Jacquier, B. *Phys. Rev. B* **1997**, *55*, 8240.

avalanche threshold whereas the wings of the beam induce the upconversion dynamics typical for below-threshold pumping. Therefore the populations N_i in eq 2 were integrated over contributions originating from rings of area $2\pi r \, dr$ induced by pump-photon flux density $P = P_0 e^{-r^2/r_0{}^2}$, where r stands for the distance from the pump-beam center with flux density P_0 and r_0 is the distance where P drops to P_0/e.

4.2.3. Power Dependence and Time Evolution.
To compare experimental and calculated curves, the measured power dependencies of the upconversion-luminescence intensity were used to scale the excitation-rate constant $P \cdot \sigma_1$ to the measured power for the two excitation energies.

For the 13365 cm^{-1} excitation the best agreement between measured and calculated power dependence of the steady-state upconversion luminescence intensity was obtained for an ESA to GSA cross-section ratio $\sigma_2/\sigma_1 = 600$. This ratio is compatible with the lower-limit estimate $\sigma_2/\sigma_1 > 200$ we got from the absorption spectrum. The calculated solid line in Figure 7a indeed shows a threshold power, and the height as well as the slope of the threshold nicely agree with the experimental data.

Using the same σ_2/σ_1 ratio, the time evolution of the upconversion luminescence also can be reproduced, see solid lines in Figure 8. However, the solid lines were obtained with the measured power values only up to 3.8 mW. At higher excitation power, i.e., 10 and 55 mW, the calculated curves with the correct $P \cdot \sigma_1$ are shown as dotted lines in Figure 8. Qualitatively, they nicely reproduce the inflection of the experimental rise curves, which is not present at low excitation powers. Also the observed acceleration of the rise above 10 mW is qualitatively reproduced. Quantitatively, however, the agreement is poor, the model reaching saturation at much shorter times than the data. A similar behavior was previously observed in avalanche simulations when the Gaussian intensity profile of the excitation was neglected.[30] Although we have included this excitation inhomogeneity in the simulation, we could only partially improve the simulation of the high-power transients. We ascribe the remaining differences to our approximation of using mean rate constants for the energy-transfer processes. In reality, there is a distribution of cross-relaxation rate constants a and b resulting from the distribution of $Os^{4+}-Os^{4+}$ distances in the crystal. The same is true for energy migration that preferentially runs along the shortest $Os^{4+}-Os^{4+}$ distances. For the Os^{4+} centers on the upper side of the distribution of $Os^{4+}-Os^{4+}$ distances the avalanche threshold is higher than the mean, and this will lead to a slowing down of the rise curve as observed. The approximation of only considering the energy-transfer processes a and b in Figure 2 is another simplification in our model that becomes effective at high power where the population density of the excited states becomes significant. Cross-relaxation $\Gamma_5\,(^3T_{1g}) + \Gamma_1\,(^1A_{1g}) \rightarrow \Gamma_5\,(^1T_{2g}) + \Gamma_5\,(^1T_{2g})$ as well as the ETU processes $\Gamma_1\,(^1A_{1g}) + \Gamma_4\,(^3T_{1g}) \rightarrow CT + \Gamma_1\,(^3T_{1g})$ and $\Gamma_1\,(^1A_{1g}) + \Gamma_5\,(^3T_{1g}) \rightarrow CT + \Gamma_1\,(^3T_{1g})$ act as additional relaxation processes at high power densities and thus affect the upconversion dynamics.

For the 11351 cm^{-1} excitation, a good agreement between the experimentally measured and simulated power dependence of the UC-luminescence intensity was obtained, see Figure 7b. Indeed, the calculation does not show any signature of an avalanche threshold, as observed. Also the time evolution depicted in Figure 9 is reasonably well reproduced by the solid lines calculated without any adjustable parameter. It is mainly determined by the lifetime $\Gamma_5\,(^3T_{1g})$. The observed acceleration between 5 and 50 mW is the result of the increased $\Gamma_5\,(^3T_{1g})$ population loss resulting from the $\Gamma_5\,(^3T_{1g}) \rightarrow \Gamma_1\,(^1A_{1g})$ ESA.

In view of the fact that only one parameter was varied to simulate the upconversion behavior under two different excitation energies and variable power, the overall agreement between experiment and calculation is very rewarding. It confirms that the model is essentially correct, the main contributing processes have been considered, and the parameters have been correctly fixed by independent measurements. The analysis shows how critically the phenomenon of photon avalanche depends on the interplay and competition between the relevant processes. The avalanche can only occur when the intermediate states are dominantly fed by cross-relaxation. This is only possible in systems with a very low GSA cross-section at the pumping energy. The avalanche in Cs_2ZrBr_6: Os^{4+} is only observed for $\sigma_2/\sigma_1 = 600$ at 13365 cm^{-1} excitation. For $\sigma_2/\sigma_1 = 60$ at 11351 cm^{-1} GSA is the dominant feeding process of the intermediate levels over the whole accessible power range. Apart from this major difference, the population losses of the intermediate level are bigger for 11351 cm^{-1} excitation, due to the lifetime of Γ_5 $(^3T_{1g})$ that is 30 times shorter than the lifetime of $\Gamma_4\,(^3T_{1g})$. At this 11351 cm^{-1} excitation energy it is therefore more difficult to keep the excitation within the absorption$-$cross-relaxation cycle. As soon as $\Gamma_5\,(^3T_{1g})$ relaxes to $\Gamma_4\,(^3T_{1g})$ the excitation is lost for further ESA steps. This loss process for 11351 cm^{-1} excitation is a gain process for 13365 cm^{-1} excitation, because it populates $\Gamma_4\,(^3T_{1g})$ from which the ESA to $\Gamma_1\,(^1A_{1g})$ takes place. In conclusion we can state, that the combination of different lifetimes of the involved intermediate levels with the different ESA/GSA ratios explains the totally different upconversion behavior observed at the two excitation energies.

How does the photon avalanche in Cs_2ZrBr_6:Os^{4+} compare with that in other systems? As already mentioned, the processes leading to the avalanche in Cs_2ZrBr_6:Os^{4+} are very similar to the ones described for LaF_3:Tm^{3+}.[30] Both systems rely on two cross-relaxations. Whereas the dynamics of the latter compound were analyzed within a four-level system, our system has five relevant states and thus enables a comparison between the two excitations. Other systems such as $YLiF_4$:Nd^{3+} [33] or $CsCdCl_3$: Ni^{2+} [10] can essentially be explained within the classical three-level situation. In most systems the avalanche-inducing ESA step starts from the excited state with the longest lifetime, thus stressing the importance of minimizing loss processes. In this respect, the 5d transition-metal ion system Cs_2ZrBr_6:Os^{4+} is analogous to the known 3d and 4f compounds. The long lifetimes of the intermediate states $\tau(\Gamma_5\,(^3T_{1g})) = 1.6$ ms and $\tau(\Gamma_4\,(^3T_{1g})) = 45$ ms are thus a key property for the observation of an avalanche. Their determination was nontrivial and finally achieved by using the unconventional technique described in Section 3, see also Figure 6.

The most striking difference of Cs_2ZrBr_6:Os^{4+} to all the avalanche systems described in the literature lies in the doping concentration. The samples exhibiting the photon-avalanche phenomenon are typically doped with 1% to 5% of rare-earth ions.[6] In $CsCdCl_3$:Ni^{2+} an even higher doping concentration of 10% was used.[10] Compared to these doping concentrations our concentration of 0.2% is extremely low. We do not know whether the energy-transfer processes in the title compound arise by electric multipole$-$multipole or exchange mechanisms. Both are expected to be significantly more efficient than in lanthanide systems. The extinction coefficients of the intraconfigurational d$-$d transitions in the title compound are typically an order of magnitude larger than for f$-$f transitions in lanthanides. For an electric dipole$-$dipole ET process this would increase the electronic factor by 2 orders of magnitude. Exchange-induced

---

(33) Joubert, M. F.; Guy, S.; Jacquier, B. *Phys. Rev. B* 1993, *48*, 10031.

ET relies on the overlap of the relevant orbitals. Compared to 4f the 5d orbitals have a much larger spatial extension, thus increasing the probability of ET by this mechanism over larger distances. We conclude that both types of ET mechanisms are significantly more efficient than in lanthanide systems, in agreement with the observed behavior.

5. Conclusions

We have synthesized the title compound Cs$_2$ZrBr$_6$:Os^{4+}, which exhibits light-emission properties not observed so far in any 4d and 5d transition-metal compound. Visible emission can be induced by NIR excitation, a very rare example of a photon-upconversion process outside the area of rare-earth compounds. Most surprisingly, the highest efficiency of the UC process is induced by exciting with laser wavelengths at which there is no ground-state absorption. The observed behavior can be accounted for by considering excited-state absorption and a so-called excitation avalanche as the dominant mechanisms. Both the power dependence and the time evolution of the phenomenon can be reproduced by a rate-equation model that considers the population density of five electronic states. The long lifetime of the excited states in the IR turns out to be crucial, because these states act as an excitation reservoir from which laser excitations are induced. In the chloride analogue Cs$_2$ZrCl$_6$:Os^{4+} the maximum vibrational frequency of roughly 350 cm^{-1} is significantly higher than in the title compound. Multiphonon relaxation within the spinor components of ^{3}T$_{1g}$ thus becomes dominant, and ESA steps to Γ_1 (^{1}A$_{1g}$) are not competitive.

Upconversion involving the first bromide to osmium charge-transfer state is also possible, but less efficient by orders of magnitude. This is due to an expansion of the OsBr$_6^{2-}$ complex in the CT excited state, which opens a nonradiative relaxation pathway bypassing the important emitting state around 16000 cm^{-1}. This nonradiative relaxation pathway also leads to a quenching of avalanche upconversion above 80 K. This is the main reason that Cs$_2$ZrBr$_6$:Os^{4+} will most likely never be used as an upconversion phosphor.